Original article

Investigation of the survival viability of cervical cancer cells (HeLa) under visible light induced photo-catalysis with facile synthesized WO₃/ZnO nanocomposite☆

Rasha A. AbuMousa [a], Umair Baig [b], Mohammed A. Gondal [c,*], Mohamed.A. Dastageer [c], Mohamad S. AlSalhi [d,*], Belal Moftah [e,f], Fulwah Yahya Alqahtani [g], Sultan Akhter [h], Fadilah Sfouq Aleanizy [f]

[a] Department of General Sciences, DES, Prince Sultan University, Riyadh 11586, Saudi Arabia
[b] Center for Research Excellence in Desalination, King Fahd University of Petroleum & Minerals, Saudi Arabia
[c] Laser Research Group, Physics Department & Center of Excellence in Nanotechnology, King Fahd University of Petroleum and Minerals, Dhahran 31261, Saudi Arabia
[d] Research Chair in Laser Diagnosis of Cancers, Department of Physics and Astronomy, College of Science, King Saud University, Riyadh, Saudi Arabia
[e] Biomedical Physics Department, King Faisal Specialist Hospital and Research Center, Riyadh, Saudi Arabia
[f] Medical Physics Unit, McGill University, Montreal, Canada
[g] Department of Pharmaceutics, College of Pharmacy, King Saud University, Riyadh, Saudi Arabia
[h] Electron Microscopy Unit, Institute for Research & Medical Consultations, Imam Abdulrahman Bin Faisal University, P.O. Box 1982, Dammam 31441, Saudi Arabia

ABSTRACT

The photo catalytic degradation, a proven chemical process used for the decontamination of organic/inorganic pollutants and microorganisms in water was implemented. In this work for the selective killing of cervical cancer cells (HeLa cells) by using nano-composite of ZnO (Zinc Oxide), WO₃ (tungsten oxide) and (n-WO₃/ZnO) as a photo-catalyst under the irradiation of visible light. All the three nanostructured semiconducting materials (WO3, ZnO and n-WO3/ZnO) were synthesized by facile chemical precipitation method and their morphological and optical characterization studies were carried out to elucidate the observed enhancement in the photo-catalytic killing of HeLa cancer cells with n-WO3/ZnO as a photocatalyst. After 60 min of photo-catalytic reaction with n-WO₃/ZnO as a photo-catalyst, a survival viability of HeLa cancer cells as low as 15% was achieved (nearly 85% of killing), as compared to 65% of HeLa cancer cell survival viability (nearly 35% of killing) with individual use of WO₃ and ZnO as photo-catalysts under the same irradiation and experimental conditions. This improved photo-catalytic killing of HeLa cancer cells using n-WO₃/ZnO in the visible spectral region is attributed to the enhanced visible light absorption and reduced electron hole recombination, characteristically brought about in the n-WO₃/ZnO composite material. As photo-catalytic killing of the cancer cells can be selective, localized and reasonably efficient, in principle, this method can be considered as a non-invasive targeted treatment option for killing any type of cancer cells. HeLa cells, in particular are the cervical cancer cell and the tumors in and around cervix, containing HeLa cells can be non-surgically accessed and photo-catalytically treated with appropriate photo-catalyst and light source.

* Corresponding authors.
E-mail addresses: magondal@kfupm.edu.sa (M.A. Gondal), malsalhi@ksu.edu.sa (M.S. AlSalhi).
☆ Research Chair in Laser Diagnosis of Cancers, Department of Physics and Astronomy, College of Science, King Saud University, Riyadh, Saudi Arabia.
Peer review under responsibility of King Saud University.

Production and hosting by Elsevier

1. Introduction

The cancer is a disease that virtually affects every human organ including blood, which remains to be a major cause of death in spite of worldwide fight against cancer for the last four decades (Sudhakar, 2009). Cancer is developed in human organs due to the damage of the DNA (deoxyribonucleic acid) in the cells and in most of the cases these damaged abnormal cells are killed by the immune system, failing which an uncontrolled cell division is triggered, causing irreparable affliction to the vital organs and the nearby organs and tissues (Blackadar 2016), where the cells faulty cancer migrate to new locations through blood stream and lymphatic system (Padera et al., 2016). Currently many treatment options like surgical removal, chemotherapy, radiotherapy, targeted therapy and immunotherapy are available to contain the erratic growth of cancer cells and mostly these therapies are given in combination such as DOX/AgNPs/MSN and CaNPs/siRNA/DOX (Arruebo et al., 2011, Gurunathan et al., 2018). In spite of overwhelming progress in each of the treatment method, the perfect cure and the quality of life before and after treatment still remains to be a big challenge, because most of the drug based and radiation based treatment methods cannot discriminate the cancer cells and the normal cells (Pilzecker et al., 2019). *HeLa* cancer cells are human cervical cancer cells and this cell line was established from the cervical cancer tumor taken from a cervical cancer patient, Henrietta Lacks (*HeLa*) in 1951 and also they were the first line of human cells to survive in vitro (Lucey et al., 2009).

Heterogeneous semiconductor based Photo-catalysis has been successfully used for the degradation of organic pollutants and for the decontamination of microorganisms in water (Gondal, et al., 2016a, Gondal, et al., 2016b, Khalil et al., 2011, Ilyas et al., 2017, Dhandapani et al., 2020, Micheal, et al., 2020). In this photochemical process, the electron hole charge pairs are photo-excited from the appropriate semiconducting material with the light radiation of suitable wavelength. These photo-generated charge carriers mediate the redox reaction to generate reactive oxygen species (ROS), which actually carry out the degradation and deactivation (Gondal et al., 2015, Vijilvani et al., 2019). Particularly in the case of photo-catalytic killing of microorganism, the crucial impairment is done to the cells of the microorganism by oxidizing cell membrane and DNA of the microorganism by photo-generated ROS to exterminate them (Ponnusamy et al., 2018). As the treatments of cancer are basically aimed to damage the faulty cells to contain their growth, photo-catalytic killing process applied for the microorganism can intuitively be a good treatment option for killing the cancer cells.

Monoclinic phase of WO_3 is proven to be one of the most effective and versatile photo-catalyst for certain photo-catalytic applications, owing to its favorable band gap energy (2.4 eV and 3.0 eV) that ensures its activity in the visible spectral region, besides its stability in oxidative and acidic environment and its resistance to photo corrosion (Gondal et al., 2009). However, the effective use of WO_3 is restricted by its relatively low visible light absorption and rapid recombination of photo generated electron hole pairs, which will definitely reduce the efficiency of photo-catalytic process. ZnO is another efficient photo-catalyst, whose band gap energy (3.3 eV) is closer to that of pioneering photo-catalyst TiO_2, and hence, in pure form, ZnO is active only in the UV spectral region (Gondal et al., 2007). Also like WO_3, ZnO also suffers rapid charge recombination, which is not quite conducive for the efficient photo-catalytic reaction. A photo-catalyst active in visible spectral region is preferred over the ones active in UV spectral region for two reasons: (i) in general, the photo-catalyst can make use of abundant solar radiation, whose spectral peak is in the visible region, and (ii) due to high photon energy, the UV

radiation can initiate some unintended reaction or damage, like for example, UV is harmful and prone to trigger cancer in human tissues (Lucas et al., 2019). Therefore for any prospective photo-catalytic treatment option for cancer, it is preferred to have a photo-catalyst, which is active in the visible region and also the ones that show less charge recombination after photo-excitation. In the present work, we synthesized the nanocomposite of WO_3 and ZnO (n-WO_3/ZnO) in order to harness the positive features of these two prominent photo-catalysts, in addition to make it working in the visible spectral region. Moreover, ZnO nanoparticles have been extensively used as anticancer agents, owing to its biocompatibility and cytotoxicity (Bisht and Rayamajhi, 2016).

When a semiconductor material is excited with the light of appropriate wavelength, the electron-hole pairs are generated and the photo generated electrons and hole can be trapped in the inter band or surface states from where they recombine quite rapidly (Wang et al., 2014). Synthesizing the semiconducting material with high crystallinity can reduce the defect induced inter band charge traps and also reducing the grain size of the material hence the probability of charge recombination is reduced (Wei and Honggang, 2018). Another method of inhibiting the recombination is inducing the spatial separation of electrons and hole by doping the host material either with a noble metal (formation of Schottky junction) or by making a composite with another suitable semiconductor (Gondal et al., 2015, Eshete et al., 2020). In the composite material, the band positions of the composite partners are in such a way that the photo excited electrons from the conduction band of the first semiconducting material migrate to the conduction band of the second material and also the holes migrate from the valance band of the second material to that of the first one to establish a spatial charge separation to effectively inhibit the charge recombination (Khalil et al., 2011, Gondal, et al., 2016b, Dhandapani et al., 2020).

In this work, nano structured WO_3 and the nanocomposite of WO_3 and ZnO (n-WO_3/ZnO) were synthesized and their morphological and optical characterizations were carried out using FE-SEM, TEM, diffused reflectance and photoluminescence spectra. All the three nano semiconducting materials were used as a photo-catalyst under visible light to kill *HeLa* cancer cells and the cell survival viability after the photo-catalytic reaction was estimated by measuring the fluorescence emission intensity from the dye mixed cancer cells. As many as 126 sets of experimental data with the combination of different experimental parameters (catalytic concentration and visible light irradiation time) were carried out. It was found that the cell survival viability after 60 min of photo-catalytic reaction with n-WO_3/ZnO was found to be considerably less than the cell survival viability with WO_3 and ZnO as photo-catalysts. As *HeLa* cells are related to cervical malignant tumors and by considering the easy accessible position of human cervix, the whole photo-catalytic treatment can be administered non-surgically.

2. Experimental section

2.1. Synthesis of WO_3 and ZnO/WO_3 nanocomposite

The WO_3 nanoparticles were synthesized by chemical precipitation method. For this, 8.24 g of the sodium tungstate [$Na_2(WO)_4$·$2H_2O$] (Sigma-Aldrich, Germany) was dissolved in 50 ml of deionized water and then with continuous stirring, 5 ml diluted HCl (Sigma-Aldrich, Germany) was added drop-wise to the sodium tungstate solution. With controlled and continuous stirring (600 rpm) at 25 °C for 2 h, the precursor became dense and yellow in color. The precipitate was then filtered and washed several times with deionized water (DI), and dried at 120 °C in an oven

for 3 h. Finally, WO_3 nanoparticles were calcined in a programmable furnace at 400 °C for 4 h and ground the dried precipitant into a fine powder (AbuMousa et al., 2018).

n-WO_3/ZnO was synthesized by simple precipitation method and for this, 500 mg of ZnO nanoparticle in 50 ml de-ionized water was ultra-sonicated in sonication baths to break up the agglomerated particles. Then in a separate beaker, 8.24 g of the sodium tungstate [$Na_2(WO)_4 \cdot 2H_2O$] (Sigma-Aldrich, Germany) salt was dissolved in 50 ml de-ionized water with continuous stirring. Both solutions were continuously stirred for 30 min and after homogenous dispersions were obtained, ZnO solution was decanted to the sodium tungstate solution. After mixing, 5 ml diluted HCl was added to the mixture of suspensions, and under controlled and continuous stirring (600 rpm) at 25 °C for 2 h, the precursor becomes dense and yellow in color. Then, the precipitant was filtered and washed with deionized water several times to remove acid impurities and then dried at 120 °C for 3 h. Finally, the dried precipitant was ground to a fine powder and transferred into the ceramic crucible to calcine for 4 h at 400 °C. With this approach, n-WO_3/ZnO was finally obtained in powder form.

2.2. Characterizations of synthesized materials

The absorption and diffuse reflectance spectra (DRS) for the synthesized materials were recorded using UV–VIS-NIR Spectrophotometer (JASCO, V-570) and the photoluminescence spectra were taken using Spectrofluorometer (JASCO, FP-8500) Scanning electron microscopy (INSPECT S50, FEI-Czech Republic) was operated at a voltage of 20 kV, whereas the transmission electron microscopy (TEM, FEI, Morgagni 268, Czec Republic) was carried out at 80 kV. For TEM and SEM, the samples were prepared by dropping particle dispersion onto the carbon-coated TEM grids (metallic stubs), and mounted into the microscope after air drying. Also, nano diffraction patterns in the TEM were recorded to evaluate the structure of each prepared material.

2.3. HeLa cell culture, photo-catalytic reaction and cells imaging

HeLa cells are human cervical cancer cell lines, cultured using DMEM (Dulbecco's Modified Eagle Medium), supplemented with 10% Fetal Bovine Serum (FBS) and 1% of Antibiotic-Antimycotic, and incubated in CO_2 environment at 37 °C. The cultured HeLa cells with the cell concentration of 3×10^5 cells/ml were transferred to the wells of 24-well experimental plate and incubated for 48 h to attach. HeLa sample taken in each well of the experimental plate treated with a particular photo-catalytic material of a particular concentration, and all the samples in the well plate are simultaneously irradiated with visible light to initiate photo-catalytic reaction. The HeLa cell survival viability was estimated by taking the ratio of fluorescence signal from treated and untreated samples stained with Alamar blue using SpectraMax-i3 micro-plate reader. The whole photo-catalytic experiment was repeated three times to take the average. The irradiation source was the xenon lamp with narrow band visible pass filter centered at 546 nm and the output light intensity was 30 mW/cm². BEL Inverted microscope (model: INV-100 LED; Rating: 100–230 V ac) with 40 X objective was used for taking the microscopic images of the treated and untreated cells for visual examination.

2.4. Statistical analysis

The results were obtained by using the software Graphpad InStat 6.0. One-way analysis of variance (ANOVA) was used. Data are expressed (mean ± SD) with a significance level of $p < 0.05$.

3. Results and discussions

3.1. Morphological characterizations

In the case of photo-catalysis, the shape and the size of the semiconductor material used as a photo-catalyst is one of the key material characteristics, as these morphological features have an effect on the available active sites on the catalytic surface for the reactants to interact. The shape and the size of the synthesized material, on the other hand depends on the method, material and the experimental conditions (concentrations in liquid phase, temperature, pH, presence/absence of surface modifiers, and time) used during the synthesis process. The SEM micrographs of WO_3, ZnO, and n-WO_3/ZnO synthesized by chemical precipitation method are shown in Fig. 1 in two different magnifications, where we can clearly observe that each material has a characteristic shape and size, and are all well dispersed. Both WO_3 and ZnO are predominantly spherical in shape with an average grain size of 50 nm for WO_3 and a slightly smaller size for ZnO and therefore the surface texture of n-WO_3/ZnO is visibly more compact. More resolved view of ZnO, WO_3, and n-WO_3/ZnO are presented with TEM images in Fig. 2, which provides more insight about the size and shape of the nanoparticles. It is quite clear from these images that WO_3 particles possess round and elongated shapes (Fig. 2a) with an average grain size of 48 ± 2 nm (Fig. 2b), whereas ZnO particles have round and oval shape (Fig. 2b), with an average grain size of 41 ± 2 nm. In the case of n-WO_3/ZnO, the surface compactness observed in the SEM image is substantiated in the TEM image and the grain size of this composite material is estimated to be 68 ± 2 nm.

Selected area electron diffraction (SAED) patterns taken from the TEM images of WO_3, ZnO and n-WO_3/ZnO are also presented in Fig. 2. For WO_3, the d- spacing values estimated from the prominent electron diffraction rings of the SAED pattern are 0.388 nm 0.377 nm 0.3156 nm and 0.2432 nm, which can be identified as the electron diffractions from (0 0 2), (0 2 0), (2 0 0) and (2 0 2) lattice planes of monoclinic WO_3 (JCPDS File no. 43–1035) (Zhang et al., 2016). In the case of ZnO, the estimated d-spacing from the SAED pattern are 0.2813 nm, 0.2601 nm 0.2472 nm correspond to (1 0 0), (0 0 2) and (1 0 1) lattice planes, which is the characteristics of wurzite ZnO (JCPDS File no. 43–0002) (Shatnawi et al., 2016). The SAED pattern of n-WO_3/ZnO shows the intermingling of the electron diffraction patterns from WO_3 and ZnO, which indicates the clear formation of ZnO/WO_3 nanocomposite.

3.2. Optical characterizations

Both WO_3 and ZnO are direct band gap materials with different band gap energies and when these two materials are combined to make a composite, their respective conduction and valance band energy positions are quite conducive for the separation of photo-excited charge carriers to reduce electron hole recombination. The band gap energies of WO_3, ZnO and n-WO_3/ZnO are deduced basically from their respective diffuse reflectance spectra. The reflectance in the ordinate axis of the reflectance spectrum is transformed into Kubelka Munk function ($F(R) = (1-R^2)/2R$) (Gondal et al., 2017, Rodwihok et al., 2020), which is equivalent to the absorption coefficient and this function $F(R)$ is used in the Tauc plot to estimate the band gap energy (Shatnawi et al., 2016). For a direct band gap semiconductor both the energy and momentum in the electronic transitions from valance to conduction bands are naturally conserved, unlike in the case of indirect band gap semiconductors, where the momentum conservation in the electronic transition is mediated by the lattice phonons (Han et al., 2019). For a direct band gap semiconductor the absorption coefficient (α) is related to the exciting photon energy (E_p) and band gap
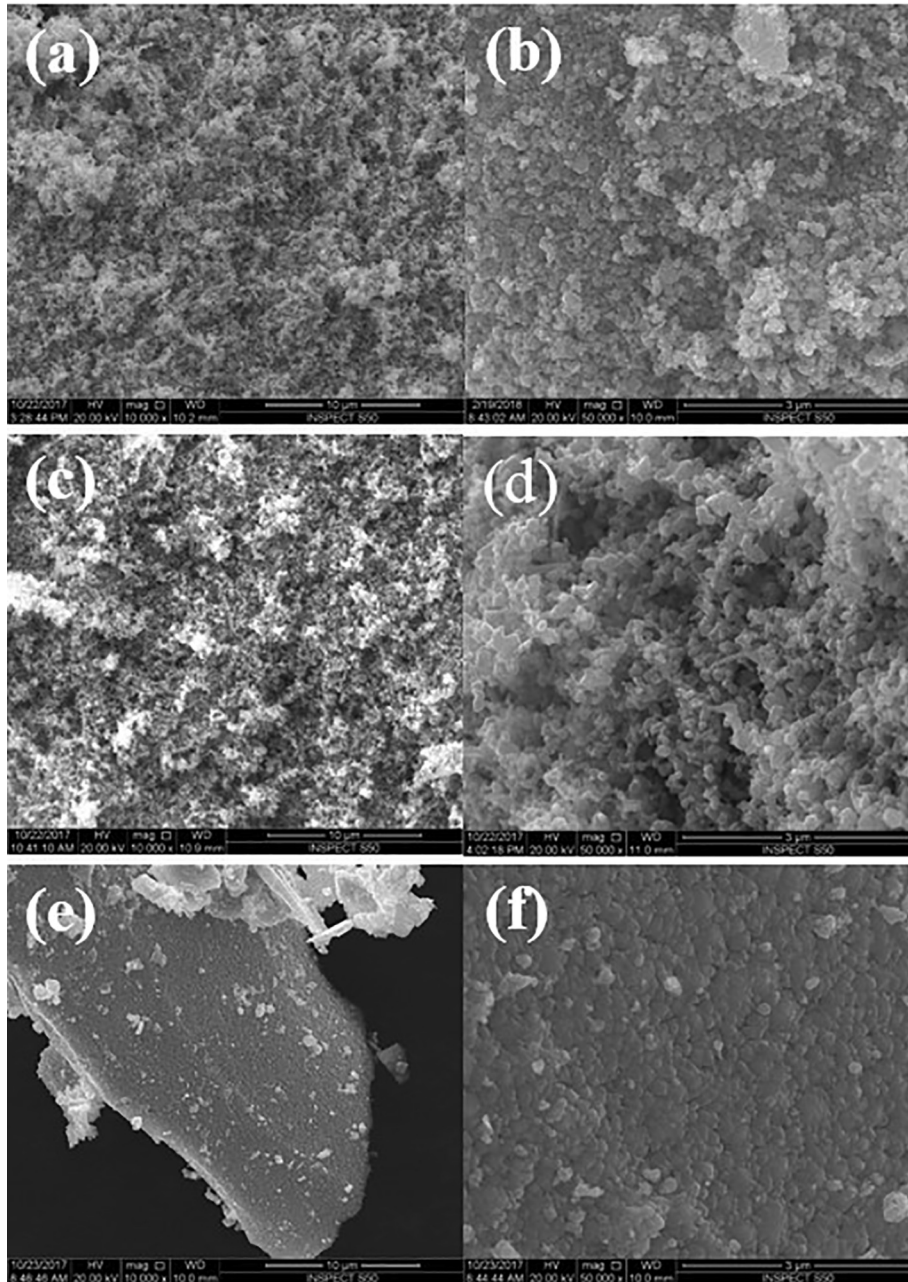
Fig. 1. SEM micrographs of the synthesized nanoparticles at a low (x10000) and a high (x50 000) magnifications for WO$_3$ (a, b), ZnO (c, d) and n-WO$_3$/ZnO (e, f).

energy (E_g) as $\alpha = A * \sqrt{E_p - E_g}$, where A is an energy independent constant, hence for a direct band gap material, $(\alpha * E_g)^2$ versus E_p plot (Tauc plot) will be linear, whose x-intercept will directly yield the band bap energy E_g. Such Tauc plots and the band gap energies for *WO$_3$*, *ZnO* and *n-WO$_3$/ZnO* are shown in Fig. 3a, where the respective band gap energies are estimated to be 2.78, 3.2, and 2.41 eV, which are in agreement with the literature (Sajjad et al., 2018). The narrowing down of the band gap energy in the *n-WO$_3$/ZnO* is attributed to the formation of oxygen vacancies with increased loading of the WO$_3$ in the mixed oxide composites (Boruah et al., 2020). Both *WO$_3$* and *ZnO* are n-type semiconductors and the composite of them becomes more n-type due to the presence of excess of unpaired electrons originating from the oxygen vacancy. Therefore in order to conserve the number of particles and to fulfill the overall electrical charge neutrality, the Fermi level has to move away from the middle of the forbidden gap towards

the conduction band, leading to the narrowing of the band gap energy.

Fig. 3b shows the absorption spectra of *WO$_3$*, *ZnO* and *n-WO$_3$/ZnO*, where we can observe the red shifting of absorption maximum and overall enhancement of the absorbance in the visible spectral region for *n-WO$_3$/ZnO*. This increased visible light activity in the composite ensures the suitability of this material to be active in the spectral peak of the abundant solar radiation. Fig. 3c is the room temperature photoluminescence spectra of the above three materials under study, excited by 325 nm wavelength. In the case of *ZnO*, the PL spectra shows two characteristic PL peaks one in the UV region, attributed to the near band edge emission and the second one in the visible region is presumably due to the electron hole recombination from the defect states (Arruebo et al., 2011). PL spectrum of *WO$_3$* has a weak emission peak at 430 nm (approximately 2.88 eV) corresponding to the emission
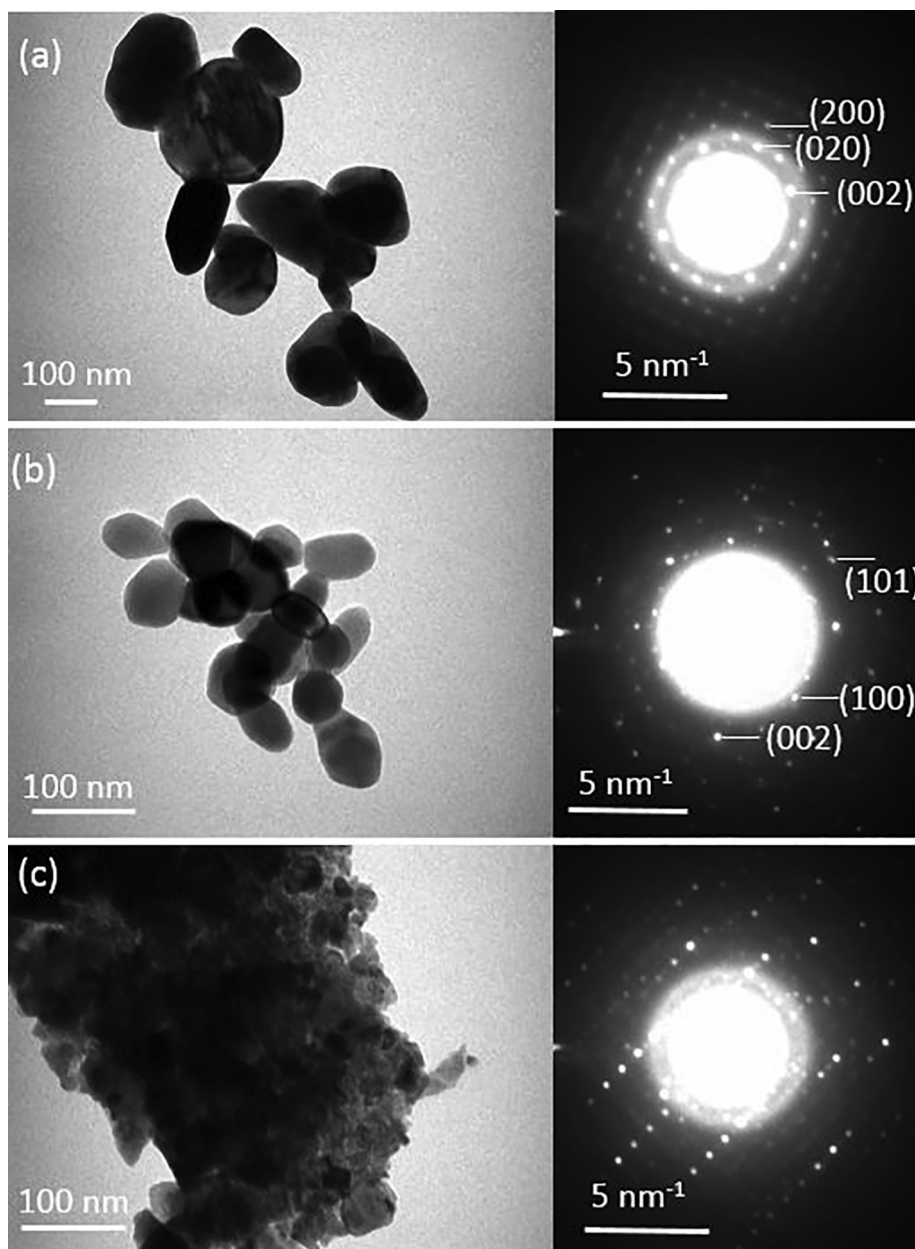
Fig. 2. TEM image of (a) WO₃, (b) ZnO and (c) *n-WO₃/ZnO* along with their SAED patterns.

due to electron hole recombination of the electrons from the lowest level of the conduction band (Staub et al., 2018). When the nano composite of *WO₃* and *ZnO* is formed, the electrons transfer from the conduction band of *ZnO* to that of *WO₃*, which is evident from the enhancement of emission (due to charge recombination) from *ZnO* at 430 nm and the absence of emission (due to charge recombination) from ZnO. More importantly we can observe an overall reduction in the charge recombination in *n-WO₃/ZnO*, which is one of the key requirements for effective photo-catalysis.

3.3. Photo-catalytic killing of HeLa cancer cells using WO₃, ZnO, and n-WO₃/ZnO

Three synthesized semiconducting materials were used as photo-catalysts under visible light for the photo-catalytic killing of *HeLa* cancer cells. The incubated *HeLa* cancer cell sample (3×10^5 cells/ml concentration) is mixed with three

photo-catalysts of 7 different concentrations (0, 0.002, 0.2, 20, 50, 100 and 200 μg/ml) and the samples were filled in 21 wells (each well for different catalytic concentration of 3 different photo-catalysts) in 24- experimental well plate, and this plate was incubated for 48 h. Six such plates were prepared; each plate is subjected to six different duration of light irradiation (5, 10, 15, 20, 30, and 60 min) with narrow band visible light (centered at 546 nm wavelength) and with the light intensity of 30 mW/cm² using a mercury lamp.

The effectiveness of the photo-catalytic killing of *HeLa* cancer cell was examined by observing the intensity of fluorescence emission from the Alamar blue stained irradiated *HeLa* cancer cells. For this fluorescence study, all the six irradiated plates containing the *HeLa* cancer cells and the photo-catalysts were stained with Alamar blue and kept in an incubator (Co₂/37 °C) for 3 h. During this process, the survived *HeLa* cancer cells convert the non-fluorescent blue colored resazurin in the Alamar blue reagent into highly fluorescing red
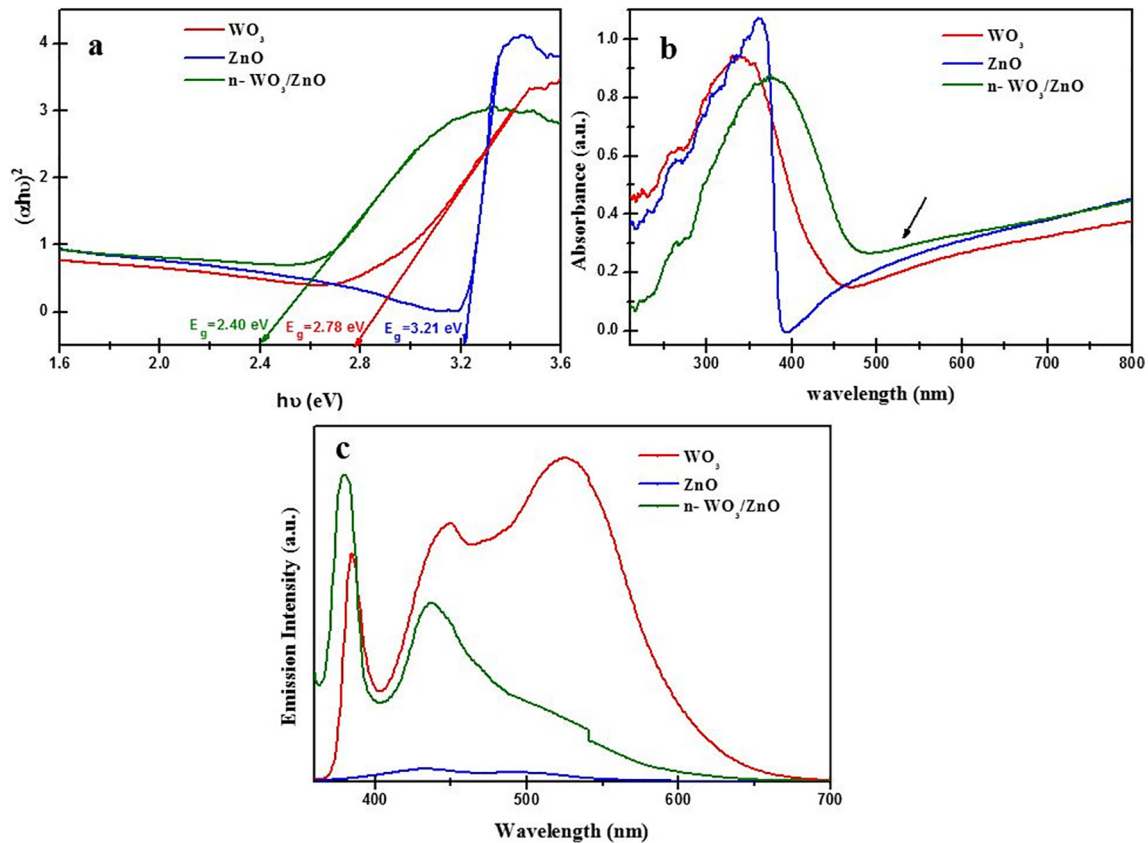
Fig. 3. (a). Tauc plot of *WO₃, ZnO*, and n-*WO₃/ZnO* with respective band gap energies. (b) Absorption spectra of *WO₃, ZnO*, and *n-WO₃/ZnO*. (c) Photoluminescence spectra at room temperature of *WO₃, ZnO*, and *n-WO₃/ZnO*.
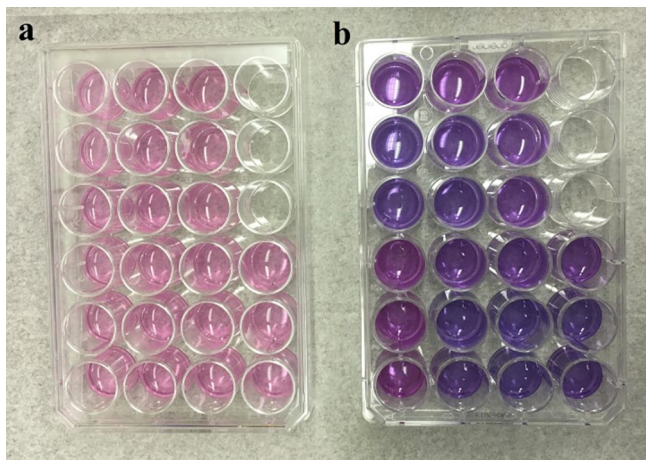

Fig. 4. (a) Alamar blue not stained and (b) Alamar blue stained.

colored resorufin (Fig. 4a), and the extent of red color transformation and consequent fluorescent intensity is proportional to the number of survived *HeLa* cancer cells (survival viability of *HeLa* cancer cells) (Fig. 4b). In this work we adopt percentage of cell survival viability described in equation (1) as a figure of merit to evaluate the photo-catalytic killing of *HeLa* cancer cells.

Cell survival viability(%)

$$= \frac{\text{Fluorecence intensity from treated cells}}{\text{Fluorecence intensity from initial untreated cells}} \times 100 \quad (1)$$

The *HeLa* cancer cell survival viability in 126 photo-catalytic experimental combinations (3 photo-catalysts × 7 catalytic concentrations × 6 irradiation durations) are summarized in Fig. 5a (*WO₃*), 5b (*ZnO*), and 5c (*n-WO₃/ZnO*). The general characteristics observed for all the three catalysts in Fig. 5 are that with the increased catalytic concentration and irradiation time, the survival viability of the *HeLa* cancer cell decreases for all the three photo-catalysts. Higher the catalyst concentration, more number of active sites is available, as a result, more number of redox reactions mediated by the photo generated charge carriers take place and this leads to the increased photo-catalytic killing of *HeLa* cancer cells. However, in general, if the catalyst concentration is beyond certain value, the solution becomes more turbid and attenuates most of the light intensity, which leads to the drop in any photo-catalytic reaction. In our case even at the highest concentration (200 μg/ml), the light attenuation effect has not set in. Also with the increased irradiation time, the number of photon available to generate the vital charge carriers by photo-excitation increases and this enhances the photo-catalytic killing of *HeLa* cancer cells.

The most important feature to be observed from the cell survival viability results presented in Fig. 5 is a remarkable reduction of cell survival viability in Fig. 5c, when *n-WO₃/ZnO* is used as a photo-catalyst. For instance, with 200 μg/ml of *n-WO₃/ZnO*, after 60 min of photo-catalytic reaction, the cancer cell survival viability has reduced to 15% (85% killing), as compared to 65% (35% killing) cell survival viability in the case of both *WO₃* and *ZnO* under the same concentration and irradiation time. This remarkable enhancement in the photo-catalytic killing of *HeLa* cancer cell due to *n-WO₃/ZnO* was brought about by the following positive features set in due to the composite formation between *WO₃* and *ZnO*: (i) As observed in the absorption spectrum in Fig. 3b, the
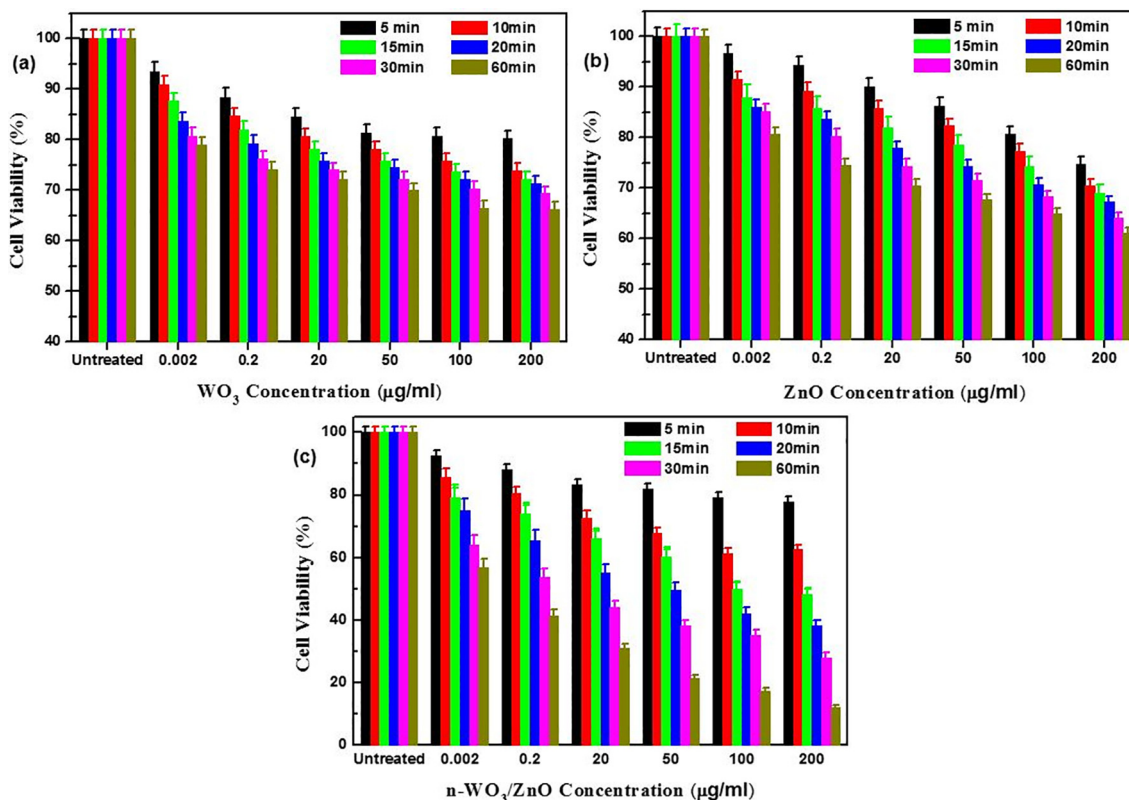
Fig. 5. Percentage of *HeLa* cell Survival viability with various concentrations of WO₃ (a), ZnO (b), and *n-WO₃/ZnO* (c) as photo-catalysts and different irradiation times. Each bar is the average of three trials and the error bars are based on standard deviations (±SD).

characteristic visible light absorption in the composite material increased, and this leads to more photo-generated charge carriers available to mediate the redox reaction to generate more reactive oxygen species (ROS) to degrade cell membrane, DNA, surface structure and cell rigidity (Baig et al., 2018). The red shifting of the absorption spectra and the enhancement of absorbance in the visible spectral region in *n-WO₃/ZnO* is due to the reorientation in the composite material and the observed reduction in the band gap energy (ii) As observed in the photoluminescence spectrum, the PL intensity for the composite material decreases, which indicates that only less number of photo-generated charge pairs are lost in the radiative charge recombination and more charge carriers are still available for effective photo-catalytic process. In the *n-WO₃/ZnO*, the spatial separation of photo-generated charge carrier takes place due to the transfer of electrons from the conduction band of *ZnO* to that of *WO₃* accompanied by the transfer of holes from the valance band of *WO₃* to that of *ZnO*, and this spatial separation of electron hole pair significantly impedes the charge recombination (Sajjad et al., 2018, Subash et al., 2013). The combined effect of enhanced visible light absorption and reduced charge recombination played out favorably to improve the photo-catalytic killing of *HeLa* cancer cells. For easy observation, a cell survival viability versus irradiation time in the photo-catalytic reaction using all three catalysts (200 μg/ml) along with the non-photo-catalytic degradation process in the absence of photo-catalyst (only light irradiation) is presented in Fig. 6, where we can observe that the killing of *HeLa* cancer cells by the light irradiation is negligible.

In addition to the photo-catalytic studies, two non-photo-catalytic experiments were carried out to study the cytotoxicity of catalysts to the *HeLa* cancer cells and also to study the effect of visible light irradiation in the killing of *HeLa* cancer cells (curve in Fig. 6). The study on the cytotoxicity of catalysts to the *HeLa*
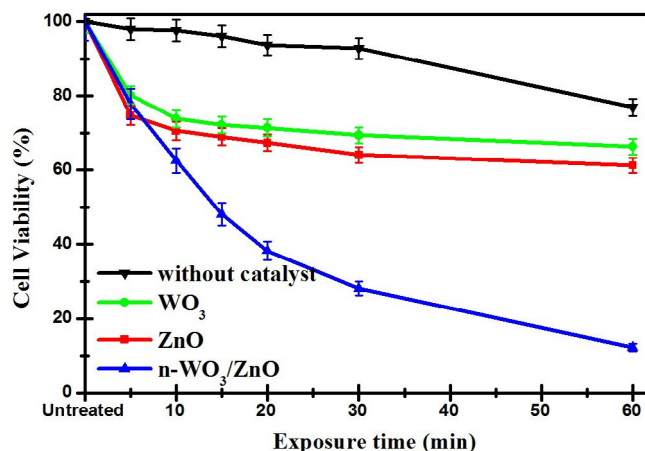

Fig. 6. The decay curves of *HeLa* cell survival viability with *WO₃*, *ZnO*, *n-WO₃/ZnO* as photo-catalysts along with the decay curve in the absence of catalyst (only light irradiation). The error bars represent the standard deviation of three trials.

cancer cells was done by keeping the *HeLa* cancer cells in the dark in the presence of WO₃ and ZnO and *n-WO₃/ZnO*, and the study on the effect of visible light irradiation in the killing of *HeLa* cancer cells was done in the absence of photo-catalysts, only subjecting the *HeLa* cancer cells to visible light irradiation of same intensity used for the photo-catalytic studies. Fig. 7 shows the cytotoxicity of catalysts to the *HeLa* cancer cells (in dark) and it is clear from the bar chart that at lower concentration (0.002 μg/mL), all the three catalysts are practically nontoxic to the *HeLa* cancer cells with the cell survival viability more than 96% in 24 h, which is in agreement with a previous study. However, when the catalyst
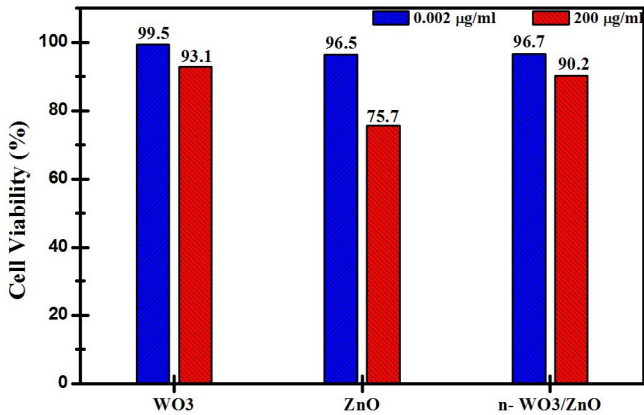
Fig. 7. Cytotoxicity of *HeLa* cancer cells represented in terms of cell survival viability treated with *WO₃, ZnO, n-WO₃/ZnO* in dark (in the absence of light irradiation).

concentration is as high as 200 μg/mL, the cell survival viability is decreased to 76%, 93%, and 90% respectively for ZnO, WO₃, and *n-WO₃/ZnO*. It should be noted from 7 that at high catalytic concentration, ZnO is more cytotoxic to the *HeLa* cancer cells than that of WO₃ and *n-WO₃/ZnO*.

3.4. Confirmation of cancer (HeLa) cell killing by image analysis

The observed photo-catalytic killing of *HeLa* cancer cells using *n-WO₃/ZnO* is visually substantiated with microscopic images in Fig. 8, where the image for the original untreated *HeLa* cancer cells is presented in Fig. 8a and photo-catalytically treated *HeLa* cancer cells are presented in 8b (20 μg/ml of *n-WO₃/ZnO* irradiated for 20 min), 8c (50 μg/ml of *n-WO₃/ZnO* irradiated for 20 min) and 8d (50 μg/ml of *n-WO₃/ZnO* irradiated for 60 min). In the microscopic image in Fig. 8a, we can see the full confluence of *HeLa* cancer cells and comparing the images in 8b, c, and d with 8a, it is quite clear that after the photo-catalytic process, a significant number of *HeLa* cancer cells were depleted and even some of the dead cells are shown with an arrow. In addition to this, Fig. 8e and 8f respectively are the images of *HeLa* cancer cells after subjecting it to visible irradiation for 60 min in the absence of

photo-catalysts and also treating the *HeLa* cancer cells with *n-WO₃/ZnO* in dark. Comparing the images in Fig. 8e and 8f with 8a, we can visibly observe that no significant change in the number of *HeLa* cancer cell is brought about by the above two non-photo-catalytic processes(AbuMousa et al., 2018).

This result further clarifies that the major killing of the *HeLa* cancer cells is carried out by the photo-catalytic process, and among the three photo-catalysts used, *n-WO₃/ZnO* is by far the best.

3.5. Mechanism of Photo-catalytic killing of HeLa cancer cells

The schematic of the mechanism that leads to the efficient photo-catalytic process involving *n-WO₃/ZnO* is shown in Fig. 9. In *n-WO₃/ZnO*, the band positions of the composite partners form a type–II heterojunction, which is optimum for the efficient spatial separation of photo-generated electron hole pairs. When the composite is irradiated with the light of appropriate wavelength, initially, the electrons are excited from the valance bands of the
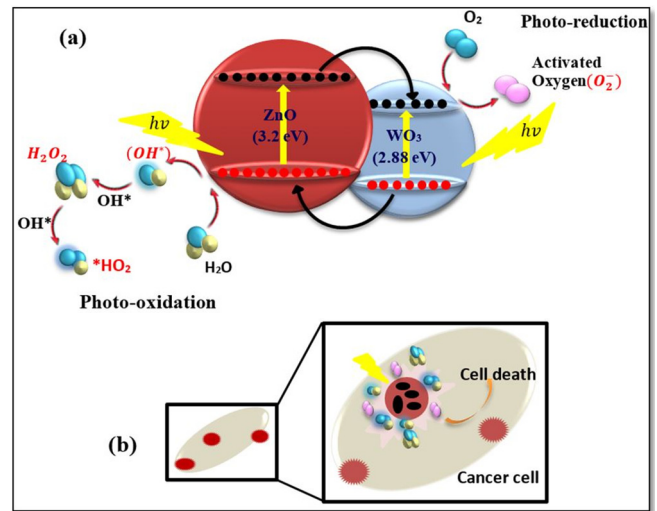

Fig. 9. Schematic diagram showing (a) the mechanism of photo-excitations, redox reactions and formation of ROS with *n-WO₃/ZnO* in water and (b) killing of *HeLa* cancer cells by ROS.

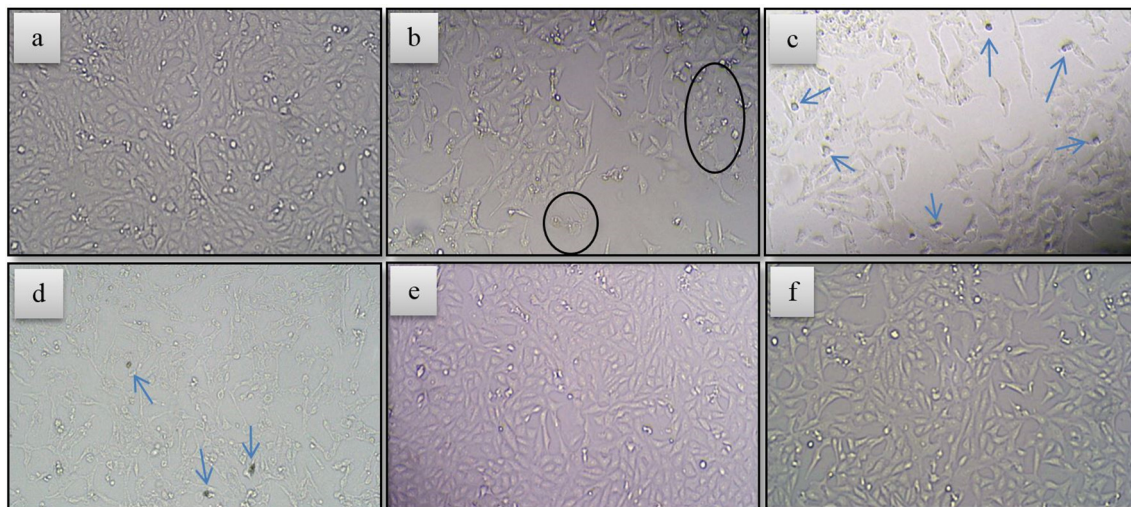**Fig. 8.** Inverted microscopic images of *HeLa* cells (Magnification 40×/0.6) for (a) original cultured and untreated cells, (b- d) cells treated with different photo-catalysts under different irradiation time, (e) cells irradiated for 60 min in the absence of photo-catalysts and (f) cells treated with 50 μg/ml of *n-WO₃/ZnO* in dark.

composite partners to their respective conduction bands (Xiao et al., 2020). In our case the electrons excited to the conduction band of *ZnO* are transferred to that of *WO₃*, while the holes are transferred from the valance band of *WO₃* to that of *ZnO*, thereby an effective spatial charge separation is established. This charge separation inhibits the recombination of electron hole pairs and makes them available for the generation of Reactive Oxygen Species ($OH^{\bullet}$, $HO_2^{\bullet}$, O_2^{-}, H_2O_2) through redox reaction according to the following chemical reactions (2–6). In aqueous environment, the photo-generated holes in the valance band oxidize the water molecule to produce hydroxyl radicals ($^{\bullet}OH$) and hydroperoxyl radicals ($OH_2^{\bullet}$), while, the electrons reduce the oxygen to produce a superoxide anion ($O_2^{\bullet-}$) or hydrogen peroxide (H_2O_2) (Baig et al., 2018).

$$O_2 + e^- \rightarrow O_2^- \tag{2}$$

$$O_2 + 2H^+ + 2e^- \rightarrow H_2O_2 \tag{3}$$

$$H_2O + h^+ \rightarrow OH^* + H^+ \tag{4}$$

$$OH^* + OH^* \rightarrow H_2O_2 \tag{5}$$

$$H_2O_2 + OH^* \rightarrow HO_2^* \tag{6}$$

These highly reactive oxygen species (ROS) reacts with the *HeLa* cancer cells to terminate them by programed cell death (apoptosis) and/or unplanned cell death (necrosis) as a result of oxidative stress (Fig. 9b). ROS reacts with the cell membrane and cell interior and affects DNA, cell rigidity and surface structure leading to the killing of *HeLa* cancer cells and these actions can be controlled by localizing the positions of the photo-catalyst at the time of light irradiation (AlSalhi, et, al., 2019, Marsooli et al., 2019). It is worth mentioning that the damage caused by ROS is more selective to cancer cells, as it is observed that the survival viability of normal healthy cell is more than 90% under the same experimental conditions corresponding to the photo-catalytic reaction that achieved 15% *HeLa* cancer cell survival viability.

4. Conclusions

Nanocomposite of *WO₃* and *ZnO* (*n-WO₃/ZnO*) were synthesized by chemical precipitation method and applied as a photo-catalyst in the process of killing cervical malignant tumor *HeLa* cancer cells in conjunction with the narrow band visible light radiation. It was found that after 60 min of photo-catalytic reaction with *n-WO₃/ZnO* as a photo-catalyst, the *HeLa* cancer cell survival viability dropped considerably compared to the cell survival viability with the individual composite partners *WO₃* and *ZnO*. The morphological and optical characterizations of the three synthesized materials were carried out and the enhancement of the photo-catalytic activity with *n-WO₃/ZnO* was explained in the light of the characterization results. The results of this work indicate that photo-catalytic killing of *HeLa* cancer cell can be considered as a localized noninvasive treatment option for cancer.

Author Contributions

M.A.G., R.A.A., U.B., M.A.D., M.S.A. and B.M. developed the concept, conceived and planned the experiments. M.A.G. and M.A.D. outlined and reviewed the manuscript. R.A.A. and U.B contributed to sample preparation, characterization, carried out the experiments, calculations and analyzed the data, wrote the manuscript. F.S.A., F.Y.A. and M.S.A. was involved in cell culture's experiments, results, and discussions. S.A. contributed in TEM and FE-SEM analysis.

Disclosers

The authors declare no competing interests.

References

Abumousa, R.A., Baig, U., Gondal, M.A., Alsalhi, M.S., umousa et al., 2018; (September):. Photo-catalytic Killing of HeLa Cancer Cells Using Facile Synthesized Pure and Ag Loaded WO₃ Nanoparticles. Sci Rep., 1–11 https://doi.org/10.1038/s41598-018-33434-7.

AlSalhi, M.S., Aziz, M.H., Atif, M., Fatima, M., Shaheen, F., Devanesan, S., Farooq, W.A., 2019. Synthesis of NiO nanoparticles and their evaluation for photodynamic therapy against HeLa cancer cells. J. King Saud Univ. – Sci. https://doi.org/10.1016/j.jksus.2019.11.033.

Arruebo, M., Vilaboa, N., Sáez-Gutierrez, B., et al., 2011. Assessment of the evolution of cancer treatment therapies. Cancers. 3 (3), 3279–3330. https://doi.org/10.3390/cancers3033279.

Baig, U., Gondal, M.A., Dastageer, M.A., Khalil, A.B., Zubair, S.M., 2018. Photo-catalytic deactivation of hazardous sulfate reducing bacteria using palladium nanoparticles decorated silicon carbide: A comparative study with pure silicon carbide nanoparticles. J. Photochem. Photobiol. B. 187, 113–119. https://doi.org/10.1016/j.jphotobiol.2018.08.010.

Bisht, G., Rayamajhi, S., 2016. ZnO nanoparticles: a promising anticancer agent. Nanobiomedicine. 3, 3–9. https://doi.org/10.5772/63437.

Blackadar, C.B., 2016. Historical review of the causes of cancer. World J Clin Oncol. 7 (1), 54–86. https://doi.org/10.5306/wjco.v7.i1.54.

Boruah, P., Khanikar, R., Heremba, B., 2020. Synthesis and Characterization of Oxygen Vacancy Induced Narrow Bandgap Tungsten Oxide (WO3−x) Nanoparticles by Plasma Discharge in Liquid and Its Photocatalytic Activity. Plasma Chemistry and Plasma Processing. https://doi.org/10.1007/s11090-020-10073-3.

Dhandapani, P., Prakash, A.A., AlSalhi, M.S., Maruthamuthu, S., Devanesan, S., Rajasekar, A., 2020. Ureolytic bacteria mediated synthesis of hairy ZnO nanostructure as photocatalyst for decolorization of dyes. Mater. Chem. Phys. 122619. https://doi.org/10.1016/j.matchemphys.2020.122619.

Eshete M, Yang L, Sharman E, Li X, Wang X, Zhang G, Jiang J. Enabling Efficient Charge Separation for Optoelectronic Conversion via an Energy-Dependent Z-Scheme n-Semiconductor-Metal-p-Semiconductor Schottky Heterojunction. J. Phys. Chem. Lett. 2020, 10.1021/acs.jpclett.0c00754

Gurunathan, S., Kang, M., Qasim, M., Kim, J., 2018. Nanoparticle-Mediated Combination Therapy : Two-in-One Approach for Cancer. Int. J. Mol. Sci. 19 (3264), 1–37. https://doi.org/10.3390/ijms19103264.

Gondal, M.A., Sayeed, M.N., 2007. Laser-enhanced photocatalytic degradation of organic pollutants from water using ZnO semiconductor catalyst. J. Environ. Sci. Health, Part A 43 (1), 70–77. https://doi.org/10.1080/10934520701750132.

Gondal, M.A., Dastageer, M.A., Khalil, A., 2009. Synthesis of nano-WO3 and its catalytic activity for enhanced antimicrobial process for water purification using laser induced photo-catalysis. Catal. Commun. 11 (3), 214–219. https://doi.org/10.1016/j.catcom.2009.10.011.

Gondal, M.A., Dastageer, M.A., Khalil, A.B., Rashid, S.G., Baig, U., 2015. Photo-catalytic deactivation of sulfate reducing bacteria–a comparative study with different catalysts and the preeminence of Pd-loaded WO3 nanoparticles. RSC Adv. 5 (63), 51399–51406. https://doi.org/10.1039/C5RA10094A.

Gondal, M.A., Ilyas, A.M., Baig, U., 2016a. Pulsed laser ablation in liquid synthesis of ZnO/TiO2 nanocomposite catalyst with enhanced photovoltaic and photocatalytic performance. Ceram. Int. 42 (11), 13151–13160. https://doi.org/10.1016/j.ceramint.2016.05.104.

Gondal, M.A., Ilyas, A.M., Baig, U., 2016b. Facile synthesis of silicon carbide-titanium dioxide semiconducting nanocomposite using pulsed laser ablation technique and its performance in photovoltaic dye sensitized solar cell and photocatalytic water purification. Appl. Surf. Sci. 378, 8–14. https://doi.org/10.1016/j.apsusc.2016.03.135.

Gondal, M.A., Dastageer, M.A., Oloore, L.E., Baig, U., 2017. Laser induced selective photo-catalytic reduction of CO2 into methanol using In2O3-WO3 nano-composite. J. Photochem. Photobiol. A Chem. 343, 40–50. https://doi.org/10.1016/j.jphotochem.2017.04.016.

Han, B., Popo, A.L., Shekunova, T.O., et al., 2019. Highly Crystalline WO3 Nanoparticles Are Nontoxic to Stem Cells and Cancer Cells. J. Nanomater. 5384132. https://doi.org/10.1155/2019/5384132.

Ilyas, A.M., Gondal, M.A., Yamani, Z.H., Baig, U., 2017. Facile synthesis of titanium dioxide-cadmium sulfide nanocomposite using pulsed laser ablation in liquid and its performance in photovoltaic and photocatalytic applications. Int. J. Energy Res. 41 (10), 1422–1435. https://doi.org/10.1002/er.3721.

Khalil, A., Gondal, M.A., Dastageer, M.A., 2011. Augmented photocatalytic activity of palladium incorporated ZnO nanoparticles in the disinfection of Escherichia coli

microorganism from water. Appl. Catalysis A. 402 (1), 162–167. https://doi.org/10.1016/j.apcata.2011.05.041.

Lucey, B.P., Nelson-Rees, W.A., Hutchins, G.M., 2009. Henrietta Lacks HeLa cells, and cell culture contamination. Arch. Pathol. Lab. Med. 133 (9), 1463–1467. https://doi.org/10.1043/1543-2165-133.9.1463.

Lucas, R.M., Yazar, S., Young, A.R., Norval, M., de Gruijl, F.R., Takizawa, Y., Rhodes, L. E., Sinclair, C.A., Neale, R.E., 2019. Human health in relation to exposure to solar ultraviolet radiation under changing stratospheric ozone and climate. Photochem. Photobiol. Sci. 18, 641–680. https://doi.org/10.1039/C8PP90060D.

Micheal, K., Ayeshamariam, A., Devanesan, S., Bhuvaneswari, K., Pazhanivel, T., AlSalhi, M.S., 2020. Aljaafreh MJ. Environmental friendly synthesis of carbon nanoplates supported ZnO nanorods for enhanced degradation of dyes and organic pollutants with visible light driven photocatalytic performance. J. King Saud Univ. – Sci. 32, 1081–1087. https://doi.org/10.1016/j.jksus.2019.10.003.

Marsooli M, Ramandi M, Adib K, Pourmasoud S, Ahmadi F, Ganjali M, Nasab A, Nasrabadi M, Plonska-Brzezinska M. Preparation and Characterization of Magnetic Fe3O4/CdWO4and Fe3O4/CdWO4/PrVO4Nanoparticles and Investigation of Their Photocatalytic and Anticancer Properties onPANC1 Cells. Materials. 2019;(October). 10.3390/ma12193274.

Padera, T.P., Meijer, E.F., Munn, L.L., 2016. The Lymphatic System in Disease Processes and Cancer Progression. Annu Rev Biomed Eng. 11 (18), 125–158.

Pilzecker, B., Buoninfante, O.A., Jacobs, H., 2019. DNA damage tolerance in stem cells, ageing, mutagenesis, disease and cancer therapy. Nucleic Acids Res. 47 (14), 7163–7181.

Ponnusamy, R., Chakraborty, B., Rout, C.S., 2018. Pd-Doped WO3 Nanostructures as Potential Glucose Sensor with Insight from Electronic Structure Simulations. J Phys Chem B. 122 (10), 2737–2746. https://doi.org/10.1021/acs.jpcb.7b11642.

Rodwihok C, Wongratanaphisan D, Tam T, Choi W, Hur S, Chung J. Cerium-Oxide-Nanoparticle-Decorated Zinc Oxide with Enhanced Photocatalytic Degradation Of Methyl Orange. Appl. Sci. 2020; 10, 1697; 10.3390/app10051697.

Sajjad, A.K.L., Sajjad, S., Iqbal, A., 2018. ZnO/WO3 nanostructure as an efficient visible light catalyst. Ceram. Int. 44 (8), 9364–9937. https://doi.org/10.1016/j.ceramint.2018.02.150.

Shatnawi, M., Alsmadi, A.M., Bsoul, I., Salameh, B., Mathai, M., Alnawashi, G., Alzoubi, G.M., Al-Dweri, F., Bawaaneh, M.S., 2016. Influence of Mn doping on the magnetic and optical properties of ZnO nanocrystalline particles. Results Phys. 6, 1064–1071. https://doi.org/10.1016/j.rinp.2016.11.041.

Singh, P., Kumar, R., Singh, R.K., 2020. Fabrication of Co- and Ce-doped ZnO nanoparticles: a structural, morphological and optical properties investigation. Appl. Nanosci. 10, 1231–1241. https://doi.org/10.1007/s13204-019-01217-9.

Staub, F., Rau, U., Kirchartz, T., 2018. Statistics of the Auger Recombination of Electrons and Holes via Defect Levels in the Band Gap—Application to Lead-Halide Perovskites. ACS Omega. 3 (7), 8009–8016. https://doi.org/10.1021/acsomega.8b00962.

Subash, B., Krishnakumar, B., Swaminathan, M., Shanthi, M., 2013. Enhanced photocatalytic performance of Ag–ZnO for Acid Black 1 degradation by UV-A light. J Mol Catal A-Chem. 366, 54–63. https://doi.org/10.1016/j.molcata.2012.09.008.

Sudhakar, A., 2009. History of cancer, ancient and modern treatment methods. J. Cancer Sci. Ther. 1 (2), 1–4. https://doi.org/10.4172/1948-5956.100000e2.

Vijilvani, C., Bindhu, M.R., Frincy, F.C., AlSalhi, M.S., Sabitha, S., Saravanakumar, K., Devanesan, S., Umadevi, M., Aljaafreh, M.J., Atif, M., 2019. Antimicrobial and catalytic activities of biosynthesized gold, silver and palladium nanoparticles from Solanum nigurum leaves. Photoch Photobio B. 111713. https://doi.org/10.1016/j.jphotobiol.2019.111713.

Wang, H., Zhang, L., Chen, Z., Hu, J., Li, S., Wang, Z., Liu, J., Wang, X., 2014. Semiconductor heterojunction photocatalysts: design, construction, and photocatalytic performances. Chem. Soc. Rev. 43, 5234–5244. https://doi.org/10.1039/C4CS00126E.

Wei, Z., Honggang, F., 2018. Defect-mediated electron–hole separation in semiconductor photocatalysis. Inorg. Chem. Front. 5, 1240–1254. https://doi.org/10.1039/C8QI00122G.

Xiao, X., Liang, S., Zhao, Y., Huang, D., Xing, B., Cheng, Z., Lin, J., 2020. Core–shell structured 5-FU@ZIF-90@ZnO as a biodegradable nanoplatform for synergistic cancer therapy. Nanoscale. 12, 3846–3854. https://doi.org/10.1039/C9NR09869K.

Zhang, N., Chen, C., Mei, Z., Liu, X., Qu, X., Li, Y., Li, S., Qi, W., Zhang, Y., Ye, Jinhua, Vellaisamy, A.L.R., Ma, R., 2016. Monoclinic Tungsten Oxide with 100 Facet Orientation and Tuned Electronic Band Structure for Enhanced Photocatalytic Oxidations. ACS Appl. Mater. Interfaces. 8 (16), 10367–10374. https://doi.org/10.1021/acsami.6b02275.